Journal Pre-proofs

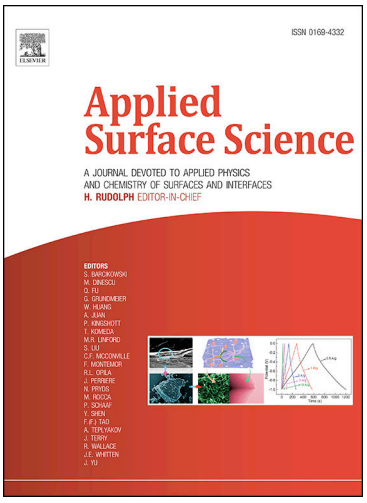

Full Length Article

Understanding promoter effects in Cr/ZrO_2 catalysts for PDH: Influence of promoters, optimum promoter-to-Cr ratio, loading sequence, and ability to re-generate

Rajvikram Singh, Raghvendra Singh, Goutam Deo

PII: S0169-4332(26)01746-0
DOI: https://doi.org/10.1016/j.apsusc.2026.167542
Reference: APSUSC 167542

To appear in: *Applied Surface Science*

Received Date: 12 March 2026
Revised Date: 8 June 2026
Accepted Date: 13 June 2026

Please cite this article as: R. Singh, R. Singh, G. Deo, Understanding promoter effects in Cr/ZrO_2 catalysts for PDH: Influence of promoters, optimum promoter-to-Cr ratio, loading sequence, and ability to regenerate, *Applied Surface Science* (2026), doi: https://doi.org/10.1016/j.apsusc.2026.167542

Understanding promoter effects in Cr/ZrO2 catalysts for PDH: Influence of promoters, optimum promoter-to-Cr ratio, loading sequence, and ability to regenerate

Rajvikram Singh, Raghvendra Singh and Goutam Deo*

Department of Chemical Engineering

Indian Institute of Technology Kanpur

Kanpur, 208016, INDIA

*** Corresponding author: goutam@iitk.ac.in**

Abstract

Propane dehydrogenation (PDH) is a key route for sustainable C_3H_6 production, where catalyst composition and preparation critically govern performance. Herein, we systematically investigate ZrO_2-supported Cr catalysts promoted with alkali and alkaline earth metals (Na, Mg, K, and Ca). Among the promoters, K exhibits the strongest promotional effect and is optimized across different Cr-loadings. While the optimal K/Cr molar ratio varies with Cr-loading, the absolute optimal K-amount remains constant (~0.11 wt.% relative to ZrO_2). XPS analysis reveals that K interacts with the ZrO_2 support, generating low-valent ZrO_X species, enabling the trapped and catalytically inactive Cr^{+3} species to reducible and PDH-active Cr^{+6} species. Based on these results, we propose a promotional model. The influence of Cr and K loading sequence on catalytic performance was also examined; and negligible effects are observed. The optimized catalyst is further evaluated over a range of contact times for both PDH and CO_2-ODH. At the highest contact time ($37.34\ g_{cat}{\cdot}h{\cdot}mol^{-1}$), the 29.46% C_3H_8 conversion and 27.15% C_3H_6 yield during PDH, significantly outperforms the 17.53% conversion and 15.52% yield observed during CO_2-ODH. These results highlight the critical role of K promotion and rational Cr-based catalyst design for efficient and sustainable propene production in industrial alkane dehydrogenation.

Keywords

PDH; CO_2-ODH; Promoter effect; K/Cr molar ratio; K-promotion model; Impregnation sequence

1. Introduction

Propene, C_3H_6, is the second most important petrochemical feedstock, and its demand continues to rapidly increase. However, the supply through conventional routes, such as refinery FFC and steam cracking, are not increasing at the same rate. Such a disparity between supply and demand is likely to contribute to the inflation of C_3H_6 prices [1]. To address this disparity there are a few on-purpose processes which are in operation to produce C_3H_6. Direct propane (C_3H_8) dehydrogenation (PDH) is one of the on-purpose processes, which contributes a significant share (~50%) towards on-purpose C_3H_6 production [1].

Chromium oxide (chromia) based heterogeneous catalyst are extensively studied for the PDH reaction since the pioneering work by Frey and Hupke [2]. Based on this study several

industries and technologies were developed [3–6]. A few strategies have been used to improve upon the catalytic activity of the supported chromia catalysts. These strategies include the use of additives and promoters, such as Sn, Zn, Ni, Ce, K, Na and others [7–15]. Specifically, alkali metals have been extensively used to promote the activity of the supported chromia catalysts. Furthermore, K is often the promoter of choice in the synthesis of efficient Al_2O_3 supported PDH catalysts. Notably, K is a versatile element in catalysis, functioning either as a promoter-as in PDH, CO_2-ODH, and RWGS reactions-or as the principal active species, as exemplified by the Dow Chemical K-MoS_2 catalyst [16–18]**.** Using K as a promoter often results in the expected neutralization of acidic sites on the catalyst, thereby lowering its overall acidity. This reduction in acidity appears to be beneficial for enhancing the resistance of the catalyst to coking during PDH [12–15].

For these promoted catalysts, there appears that at a certain promoter-atom to Cr molar ratio the catalyst shows the highest activity and changing the ratio reduces the catalytic activity [19]. However, the effect of Cr-loading on the best promoter-atom/Cr molar ratio is not addressed. Such a study will be useful to improve our understanding of the role of the promoter, which in future can be helpful in the synthesis and design of the catalyst. Furthermore, the effect of promoters is usually undertaken for Al_2O_3 supported chromia catalysts [10,19–23]. However, previous studies reveal that ZrO_2 supported chromia catalysts show better turn-over frequency (TOF) for PDH than Al_2O_3 supported catalysts [24–26]. A comparative study of different alkali and alkaline promoters on ZrO_2 supported chromia catalysts appears to be limited to the choice of K as the promoter [27–29]. For example, it was shown that addition of K to a ZrO_2 supported chromia catalyst leads to a decrease in acidity of the catalyst. Furthermore, the initial activity of the catalyst decreases and the selectivity towards C_3H_6 improves when K is added [28]. The decrease in activity appears to be contrary to the promotional effect of K addition.

Moreover, in these multicomponent systems, the sequence of impregnation of the different components on the support, such as co-impregnation or sequential impregnation of the precursors, may play an important role. A previous study has shown the effect of sequence of impregnation of Cr and K on an Al_2O_3 support [23]. This study shows that there is no effect on conversion of C_3H_8 due to sequence of impregnation, though the selectivity of C_3H_6 increases by 5% if K was impregnated before the Cr. A similar study on ZrO_2 supported chromia catalyst appears to be missing.

In addition to the above, the catalysts used in the PDH process tend to deactivate within a short operational period, necessitating periodic regeneration [23]. The ability of the catalyst to regenerate itself after multiple cycles is a critical attribute. Although previous studies have demonstrated that catalysts can recover their initial activity after the first regeneration cycle, a gradual decline in performance is typically observed over successive cycles, indicating a loss of long-term catalytic stability [9,11,26,30–33]. The causes for deactivation and ability of the catalyst to recover its original activity over successive regeneration cycles are important factors that also needs to be addressed.

With recent advances in CO_2 utilization, it has been suggested to use CO_2 as an oxidant during the PDH reaction [34,35]. The resulting CO_2-ODH of C_3H_8 reaction has also been examined in several studies [4,36,37]. The primary advantage includes the utilization of CO_2, whereas the primary disadvantage includes the loss of H_2 produced due to the simultaneously occurring reverse water gas shift reaction taking place [38]. However, studies comparing the PDH and CO_2-ODH reaction over ZrO_2 supported chromia catalysts are limited [34,35,39].

Thus, the lack of information on examining the effect of: (i) using different alkali and alkaline promoters, (ii) Cr-loading on the best promoter/Cr molar ratio, and (iii) the sequence of impregnation of Cr and promoter for ZrO_2 supported chromia catalyst highlights the need for further investigation in this area. Furthermore, the ability to regenerate and comparison of the catalytic PDH and CO_2-ODH processes needs to be addressed. These form the primary objective of the present study.

To achieve our objectives, we investigate the influence of various alkali and alkaline metal promoters on ZrO_2 supported chromia catalyst, with the initial objective of identifying the most effective promoter amongst Na, K, Mg and Ca. Upon selecting the most effective promoter, we examine its interaction with three different Cr-loadings to determine the most suitable promoter-atom/Cr molar ratio for each Cr-loading. Subsequently, we explore the impact of the synthesis sequence on the performance of the most effective promoted catalyst. Based on our results we propose a model to explain the role of the promoter and how promotion works in ZrO_2 supported Cr catalysts. Then we carry out a multiple-regeneration study to evaluate the regenerative capacity of the catalyst across successive regeneration cycles. Finally, using the most active promoted and unpromoted ZrO_2 supported chromia catalyst, we compare PDH and CO_2-ODH under the same operating conditions.

2. Experimental procedure

2.1. Catalyst synthesis

All the three set of catalyst samples were synthesized by the incipient wetness impregnation method and calcined in presence of air [27]. The first set of catalysts were synthesized to examine the effect of different alkali and alkaline promoters for ZrO_2 supported chromia catalyst. The promoters comprise, Na, K, Mg and Ca. The effect of these promoters was examined over 1wt.% Cr catalyst supported on zirconia (ZrO_2, *Saint Gobain*) and the most effective promoter was identified. The precursor used for all the metals were: Cr - chromium nitrate nonahydrate ($Cr(NO_3)_3.9H_2O$, *Sigma Aldrich*), Na - sodium nitrate ($NaNO_3$, *Sigma Aldrich*), K - potassium nitrate (KNO_3, *Sigma Aldrich*), Mg - magnesium nitrate hexahydrate ($Mg(NO_3)_2.6H_2O$, *Sigma Aldrich*) and Ca - calcium nitrate tetrahydrate ($Ca(NO_3)_2.4H_2O$, *Sigma Aldrich*). All the catalysts are prepared in the same molar ratio of A/Cr, where A = Na, K, Mg or Ca.

Based on the most effective promoter, the second set of catalysts were synthesized. This set of catalysts were prepared to determine the best promoter-atom/Cr molar ratio for different sub-monolayer and near-monolayer loadings of chromia (1 wt. % Cr, 1.5 wt. % Cr, and 2.5 wt. % Cr). Of the three metal loadings chosen the best promoter-atom/Cr ratio was already determined for Cr = 2.5% in our previous study [27].

For the third set of catalysts the sequence of impregnation was examined for the most effective catalysts. In this set three catalysts were compared: one catalyst was synthesized where Cr and the promoter-atom were co-impregnated on the support, in the second catalyst Cr was initially deposited on the ZrO_2 support followed by the promoter-atom, and in the third catalyst the promoter-atom was initially deposited followed by Cr. For a Cr-loading of 2.5 and a K/Cr ratio of 0.05 the catalysts chosen for examining the sequence of impregnation were: 2.5Cr0.05K, $2.5Cr_1 0.05K_2$ and $2.5Cr_2 0.05K_1$. The latter two catalysts differed in the sequence with which Cr and K were impregnated to the pre-treated ZrO_2 support, where the subscripts 1 and 2 denote the component that was deposited first and the one deposited second.

2.2. Catalyst characterization

2.2.1. Surface area measurement and elemental composition

The specific surface area of the catalyst samples was measured by using multi point BET method. The measurements were carried out on an Autosorb iQ TPX equipment (Quantachrome, USA), using N_2-adsorption data at -196℃. The degassing of the samples was performed at 150℃ for 6 h, and the amount of sample used was ~200 mg.

The elemental composition of selected samples was analysed to verify their conformity with the expected (nominal) values using energy-dispersive X-ray spectroscopy (EDS). The analysis was performed with an integral EDS detector attached to a Quanta 200 field emission scanning electron microscope (JEOL, Japan). The microscope operated at an accelerating voltage of 15.0 kV and a magnification of 250X. Prior to EDS measurements, a thin gold layer was deposited, using a JEC 300 gold sputter coater (JEOL, Japan) to minimize surface charging during imaging.

2.2.2. UV-vis spectroscopy

The UV-vis spectra of all the samples were obtained under ambient conditions using a UV-vis-NIR 5000 (Varian, USA) spectrometer. All the calcined samples were scanned in the range of 200-800 nm, under ambient conditions. The ZrO_2 support was employed as the reference to isolate the effects associated with changes in the chromia phase.

2.2.3. Raman spectroscopy

All the calcined and some of the spent samples were scanned using an Acton Spectra Pro 2500i instrument (Princeton Instrument, USA). A 532 nm laser was used which was operated at its 50% of its max strength of 40 mW. The 20X and 50X lenses were used to focus the laser on to the samples. All the spectra were obtained at room temperature using 20 scans of 2 second each. The samples were stationary while scanning. Thus, there is a high chance that laser induced heating occurred during collection of the Raman spectra [40].

2.2.4. X-ray photoelectron spectroscopy (XPS)

XPS measurements were carried out using a Thermo-Scientific NEXSA spectrometer equipped with a monochromatic Al Kα X-ray source (hν=1486.6 eV). The spectra were recorded under ultra-high vacuum conditions with a base pressure of ~3×10^{-9} mbar. Survey spectra were collected with a pass energy of 200 eV, while high-resolution spectra were acquired with a pass energy of 50 eV, resulting in an overall energy resolution of approximately 0.45 eV. The binding energy scale was calibrated using the C 1s peak of adventitious carbon at 284.8 eV to compensate for surface charging effects. Background subtraction was performed using a Shirley-type background. Peak deconvolution and fitting were conducted using mixed Gaussian-Lorentzian (GL) line shapes. During the fitting procedure, parameters such as peak position, full width at half maximum (FWHM), and relative peak areas were optimized while maintaining physically meaningful constraints, including appropriate spin-orbit splitting and intensity ratios where applicable.

2.2.5. H_2-TPR

The H_2-TPR studies were performed using an AMI 200 (Altamira, USA) set-up and associated software. Analysis of the H_2-TPR profile was performed using the same protocol as reported in our earlier study [27], which involved sample pretreatment, reduction under a 10% H_2-Ar

gas mixture, and effluent gas analysis using a thermal conductivity detector (TCD). From the plot between TCD signal vs bed temperature, the H_2-TPR profile was generated, and the area under this curve was the amount of H_2 consumed, which was also referred to as the H_2-uptake. The area was calibrated by using pulse calibration of the same H_2-Ar gas mixture. Based on the H_2-uptake and nominal Cr-loading the H/Cr molar ratio was calculated.

2.3. Reactivity studies

The synthesized catalysts were tested for the PDH and CO_2-ODH reactions for 2 h time-on-stream (TOS) in a down flow quartz tube backed bed reactor. The reactor was placed in a vertical tubular furnace in which the gases flowed downward. A bed of quartz wool was made to support 100 mg of fresh catalyst. To measure the temperature, a K type thermocouple was placed just above the catalyst bed. To control the temperature, the thermocouple was connected to a PID controller (OMEGA, USA). Before performing the reaction, the catalyst was calcined at 550°C for 1 h with an O_2 flowrate of 2.4 $L.h^{-1}$. For PDH, a gaseous mixture of 7.5% C_3H_8-N_2 was fed to the reactor at a rate of 1.8 $L.h^{-1}$. For CO_2-ODH a mixture of C_3H_8, CO_2 and N_2 was fed at a total flowrate of 1.8 $L.h^{-1}$, where C_3H_8 and CO_2 was fed in stoichiometric molar proportions, and the inlet partial pressure of C_3H_8 was maintained at 0.075 atm. At the exit of reactor, the outflowing gases were mixed with CH_4 at a rate of 0.12 $L.h^{-1}$ to normalize the effluent gases. This strategy was used since only trace amounts of CH_4 was formed during PDH and CO_2-ODH. This gas was passed through the condenser to remove the possibility of moisture in the gaseous mixture. All gas flow rates were controlled by mass flow controllers (Bronkhorst, Netherlands).

The gas samples were taken to analyse the exit gas composition, and it was injected to a GC (NUCON, 5700), equipped with a TCD and a flame ionization detector (FID). A HySep-Q column was used to separate the gases present in the mixture. The area of each component was determined and used to calculate the conversion of C_3H_8 ($X_{C_3H_8}$) yield of C_3H_6 ($Y_{C_3H_6}$) and selectivity of C_3H_6 ($S_{C_3H_6}$). Other reactivity parameters were also calculated, such as the turnover frequencies ($TOF_{C_3H_6}$ and $TOF_{C_3H_6}$). The formulae used for these calculations are given in equations (1) to (7).

$$X_{C_3H_8}(\%) = \left(1 - \frac{F_{C_3H_8,out}}{F_{C_3H_8,in}}\right) * 100 \quad (1)$$

$$X_{CO_2}(\%) = \left(1 - \frac{F_{CO_2,out}}{F_{CO_2,in}}\right) * 100 \quad (2)$$

$$Y_{C_3H_6}(\%) = \left(\frac{F_{C_3H_6,out}}{F_{C_3H_8,in}}\right) * 100 \quad (3)$$

$$Y_{CO}(\%) = \left(\frac{F_{CO,out}}{F_{CO_2,in}}\right) * 100 \quad (4)$$

$$S_{C_3H_6}(\%) = \left(\frac{F_{C_3H_6,out}}{F_{C_3H_8,in} - F_{C_3H_8,out}}\right) * 100 \quad (5)$$

$$TOF_{C_3H_6} = \left(\frac{F_{C_3H_6,out}}{W*H_2-uptake}\right)(s^{-1}) \quad (6)$$

$$TOF_{C_3H_8} = \left(\frac{F_{C_3H_8,in}-F_{C_3H_8,out}}{W*H_2-uptake}\right)(s^{-1}) \quad (7)$$

In equations (1) to (7), F_i is the molar flow rate of the species i, W is the mass of the catalyst, and $H_2-uptake$ is the mols of H_2 per unit mass of the catalyst. The carbon balance (%), $\frac{mol\ C_{out}}{mol\ C_{in}} * 100$, was determined for each run and was found to be better than 98%. The reaction data at each condition was repeated at least 3 times and the average and standard deviation was reported.

The most active catalyst was also tested for deactivation and regeneration for a more prolonged time-on-stream (TOS) study. During the deactivation process the reaction was carried out for 6 h and the data was collected intermittently. Subsequently, the catalyst was regenerated by switching the gas stream to an inert feed and then to an oxidizing atmosphere of pure O_2 without changing the temperature. The catalyst was oxidized for 0.5 h. After oxidation the reactor was purged and then switched to the reactant mixture and the 2nd cycle was analysed for another 6 h. This process was repeated to achieve five cycles of regeneration.

3. Result and Discussion

3.1. Surface area studies and elemental composition

The surface area of all the samples was measured and tabulated in Table S1 of the supported information file. Analysis of Table S1 reveals that the simultaneous presence of chromium and promoters do not induce any significant alteration in the specific surface area (m^2/g_{cat}). For instance, the specific surface area of the support material ZrO_2 is approximately 48 m^2/g, and all synthesized catalysts exhibit surface areas within a comparable range. Minor variations in surface area have also been reported by others [41–43].

The last set of catalysts were examined by EDS; to compare the measured amount of promoter (K) and chromium (Cr) present with the nominal amount. The result of the EDS analysis is shown in Table S2 of the supplementary information file. The measured and nominal amounts are similar, suggesting that the targeted composition of the synthesized catalysts was achieved.

3.2. UV-vis spectroscopy studies

The UV-vis spectra of all the samples are shown in Figure S1 to S5 of the supplementary information file. The spectra show two bands at 275 and 375 nm. These bands correspond to Cr^{+6} species [27,44,45]**.** However, these spectra do not show any differences with addition of promoter.

3.3. Raman spectroscopy studies

The three sets of supported metal oxide samples were characterized using Raman spectroscopy. The spectra corresponding to the 1Cr0.10A samples are shown in Figure 1, where A = Na, K, Mg, K and Ca. The spectra clearly show well-defined bands due to ZrO_2 at 476, 615, and 635 cm^{-1} [46,47]. In addition to the support peaks, 1CrZr exhibits a broad peak at 853 cm^{-1} and 1004 cm^{-1}. A shoulder at 1031 cm^{-1} is also evident. These spectra clearly indicate the presence of molecularly dispersed chromia species and absence of Cr_2O_3 species. These three peaks are

also visible in all the promoted samples. It appears that the intensity of the three peaks of the molecularly dispersed chromia species increase for A = Mg, K and Ca, but not for A = Na. For 1Cr0.1Na and 1CrZr, the intensity of the three peaks is similar.

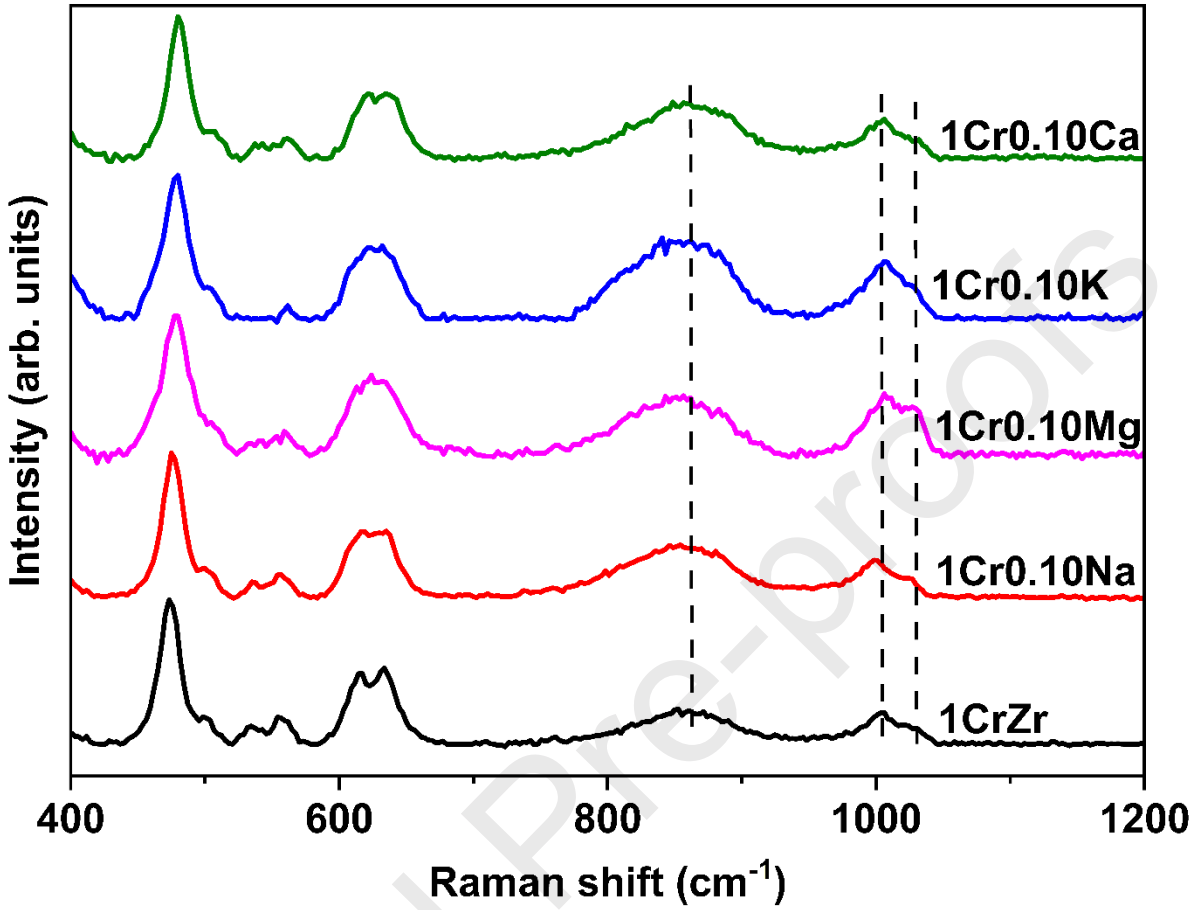

Figure 1: Raman spectra of 1CrZr and 1Cr0.10A catalyst showing the effect of different promoter addition, A = Na, Mg, K and Ca.

The Raman spectra of 1CryK, where y = 0.00, 0.05, 0.10, 0.15 and 0.20, is shown in Figure 2. The spectra also show same three distinct peaks between at ~850, 1003 and shoulder at 1027 cm^{-1}. The Raman peaks associated with crystalline Cr_2O_3 continue to be absent. Relative to the 1CrZr spectrum, the addition of K increases the intensity of the broad peak at ~850 cm^{-1}. However, to determine the quantitative variation of the intensity of the chromia peaks with change in K/Cr molar ratio is challenging.

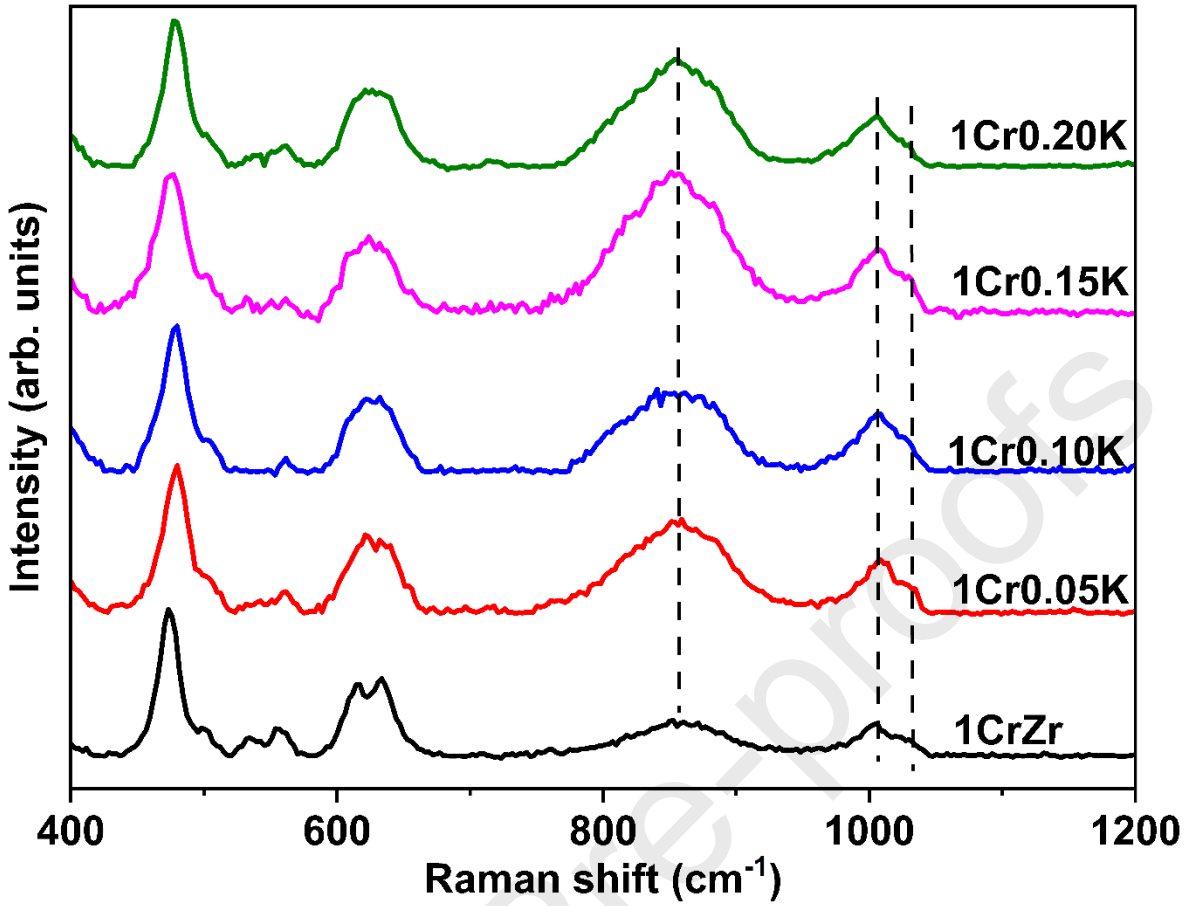

Figure 2: Raman spectra of 1CryK catalysts, showing the effect of potassium addition, y = 0.00, 0.05, 0.10, 0.15 and 0.20.

The Raman spectra of 1.5CryK, where y = 0.00, 0.05, 0.10 and 0.15, are shown in Figure S6. Similar spectra are seen for the 1.5CryK samples as those of the 1.0CryK samples. Three Raman bands are also seen at 850 (broad), 1003 and 1027 (shoulder) cm^{-1}. The Raman bands due to Cr_2O_3 continues to be absent. However, the changes in intensity of the three peaks with increase in K/Cr ratio is more evident. As the amount of K increases until the K/Cr molar ratio is 0.10, the intensity of the bands increases, and with further addition of K the intensity of bands decreases.

The Raman spectra of 2.5CryK, where y = 00, 0.05, 0.10, 0.15 and 0.20, was analysed in our previous study [27] and is reproduced in Figure S7 of the supplementary information file. The spectrum for 2.5CrZr shows a Raman band at 550 cm^{-1}, which is due to Cr_2O_3 crystallites [38]. The three Raman bands at 848, 1008 and 1031 cm^{-1} due to the surface chromia species are also present. The presence of Cr_2O_3 crystallites suggest that monolayer coverage is exceeded, as was concluded in our previous study [38]. Thus, the Cr_2O_3 crystallites and molecularly dispersed chromia species are simultaneously present at these loading of chromia. With addition of K, the intensity of the Cr_2O_3 band at ~550 cm^{-1} appears to fluctuate. A previous study suggests that $K_2Cr_2O_7$ is initially formed, which decomposes into K_2CrO_4 and α-Cr_2O_3 [48]. Analysis of the changes in intensities of the Raman bands with an increase in K is difficult, though it appears that the intensity of the band at 848 cm^{1} increases, and the intensity of the shoulder at 1031 cm^{-1} initially increases and then decreases.

The Raman spectra of the last set of catalysts are shown in Figure S8 of the supplementary information file. The KZr and 2.5CrZr are included for reference. The KZr sample shows a broad band at 850 – 1000 cm^{-1}. The remaining samples show similar Raman bands due to the

surface molecularly dispersed chromia species at 850, 1010 and 1031 cm^{-1}. It is again difficult to decipher any changes in the band intensities due to changes in impregnation method.

3.4. XPS studies

The Cr 2p XPS spectra of some freshly calcined samples were obtained. The spectra of 1CrZr, 1.5CrZr, 2.5CrZr, 1Cr0.15K, 1.5Cr0.10K, and 2.5Cr0.05K are shown in Figure 3. The presence of both Cr^{+3} and Cr^{+6} species in the spectra is evident. The 2.5CrZr sample shows an additional Cr^{+3} peak corresponding to crystalline Cr_2O_3 species, which is visible in both the $2p_{3/2}$ and $2p_{1/2}$ regions at binding energies of 577.4 eV and 587.0 eV, respectively. This observation is consistent with the Raman spectra, which show the appearance of Cr_2O_3 crystalline bands at approximately 551 cm^{-1} for Cr loadings above 2 wt.%.

The Cr^{+3} species strongly interacting with ZrO_2 in the unpromoted samples, and not due to Cr_2O_3, appear at 576.3 eV and 586.0 eV in the $2p_{3/2}$ and $2p_{1/2}$ regions, respectively. In the presence of K, these Cr^{+3} species are converted to Cr^{+6} species. In the spectra shown in Figure 3, two types of Cr^{+6} species are identified: (i) surface Cr^{+6} species, present in all samples, and (ii) K-associated Cr^{+6} species, observed predominantly at higher Cr loadings, particularly in the 2.5Cr0.05K sample [49]. The surface Cr^{+6} species appear at relatively high binding energies, which further increase with metal loading, from 577.1 eV and 587.1 eV for 1CrZr to 579.1 eV and 588.4 eV for 2.5Cr0.05K in the $2p_{3/2}$ and $2p_{1/2}$ regions, respectively. Similar trends have been reported in the literature, indicating that variations in metal loading influence the binding energies of specific chromium species [50]. An additional feature is observed in the 2.5Cr0.05K sample at 581.4 eV and 590.6 eV, which appears to be due to potassium chromate-type complexes [51].

The Zr 3d XPS spectra of the same freshly calcined samples are presented in Figure 4. All samples exhibit the characteristic peaks of Zr^{+4} (ZrO_2) at 181.5 eV ($3d_{5/2}$) and 184.3 eV ($3d_{3/2}$). Upon K addition, the emergence of lower oxidation state Zr^{+3} (ZrO_X) species is observed at 182.5 eV ($3d_{5/2}$) and 185.9 eV ($3d_{3/2}$) [52,53]. The presence of K in the supported chromia catalyst appears to generate the lower oxidation state of zirconia ZrO_X [53].

The O 1s XPS spectra of the freshly calcined samples, shown in Figure S9 of the supplementary information file, reveal three distinct oxygen species in the unpromoted catalysts. The oxygen species possesses binding energies of 529.6 eV, 530.8 eV, and 532.4 eV, corresponding to O-Zr (ZrO_2), O-Cr, and hydroxyl species, respectively [53]. The intensity of the O-Cr peak increases with Cr loading. In K-promoted samples, an additional peak appears at 531.5 eV, assigned to O-Zr in ZrO_X species, and its intensity also increases with higher metal loading.

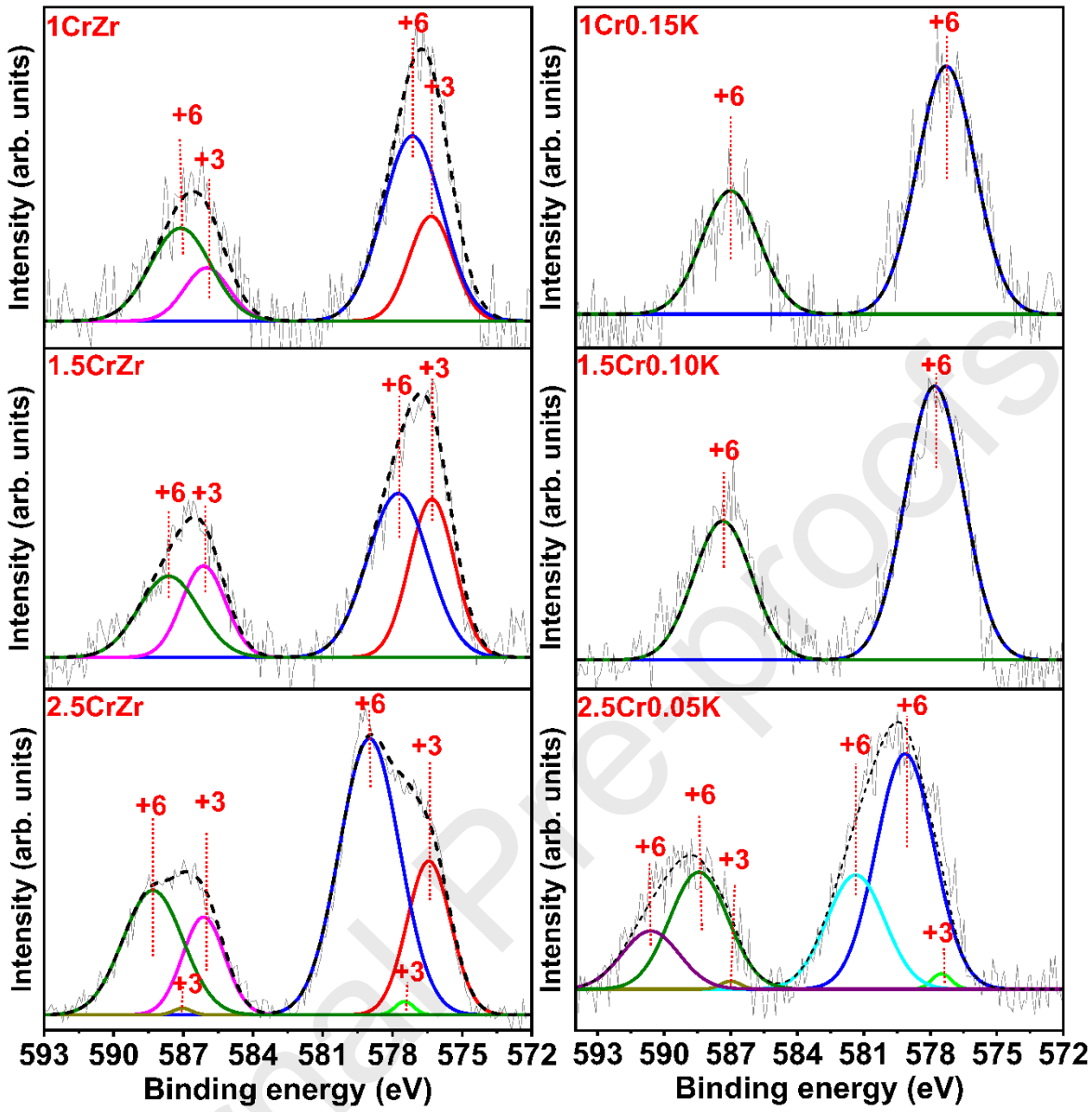

Figure 3: Cr XPS spectra of freshly calcined samples of 1CrZr, 1.5CrZr, 2.5CrZr, 1Cr0.15K, 1.5Cr0.10K and 2.5Cr0.05K

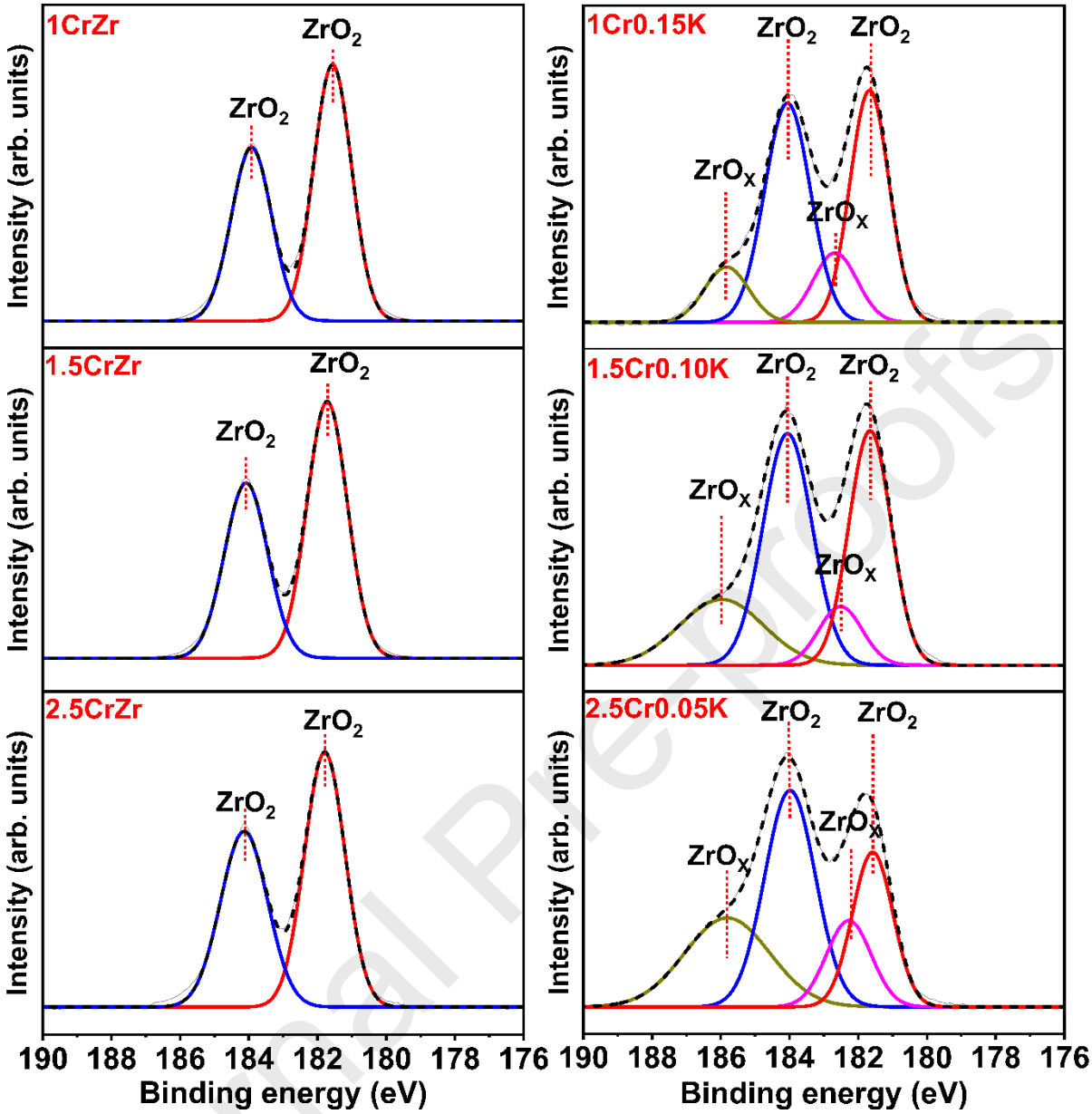

Figure 4: Zr XPS spectra of freshly calcined samples of 1CrZr, 1.5CrZr, 2.5CrZr, 1Cr0.15K, 1.5Cr0.10K and 2.5Cr0.05K

3.5. H_2-TPR studies

The H_2-TPR profiles of 1CrZr and 1Cr0.10A, are shown in Figure 5. All the samples show a single reduction peak in the H_2-TPR profile, which indicates that there is only a one-step reduction involved.

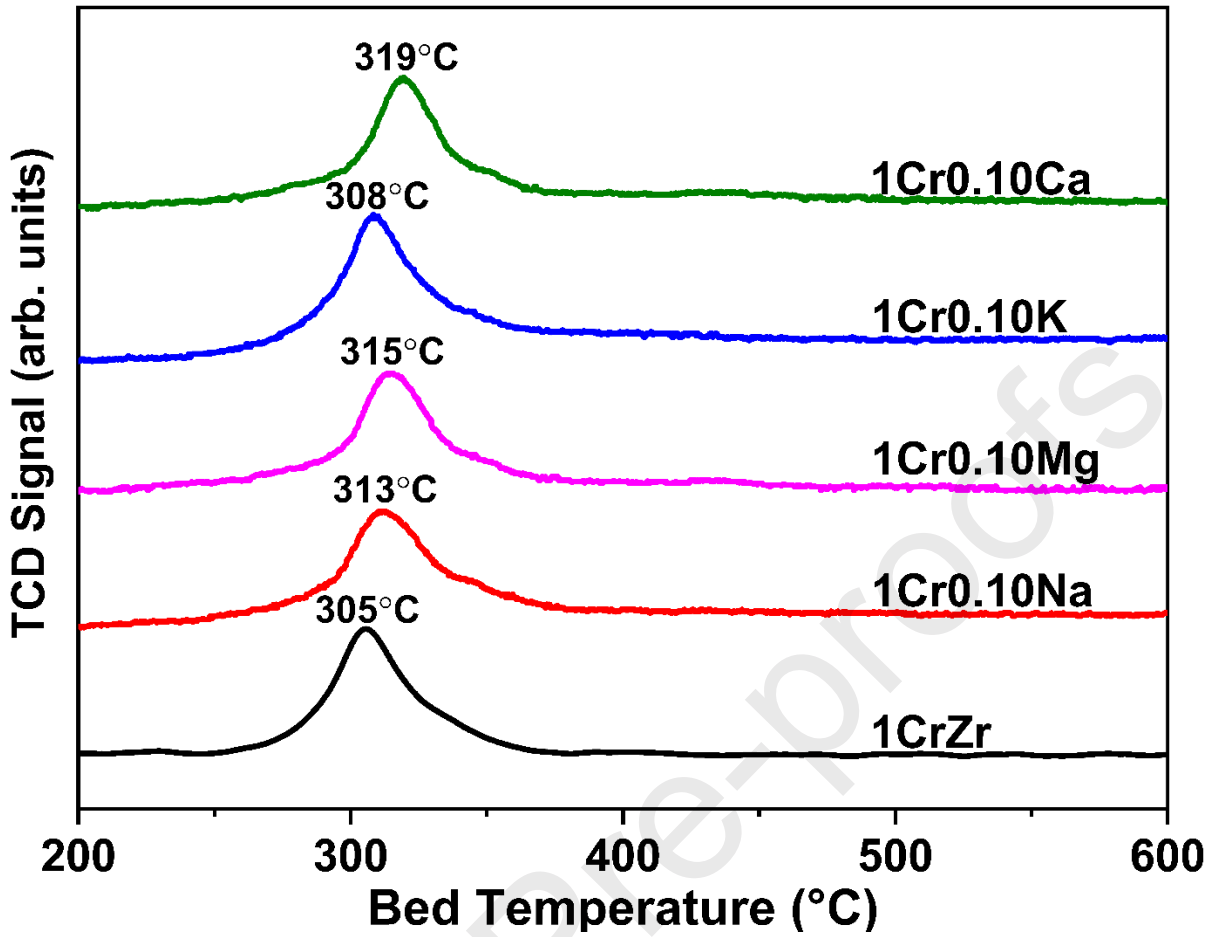

Figure 5: H_2-TPR profile of 1CrZr and 1Cr0.10A catalyst showing the effect of different promoter addition, A = Na, Mg, K and Ca.

The temperature at which the TCD current is maximum, also referred to as T_{MAX} of the sample, is also mentioned in Table 1. It was observed that the simultaneous presence of chromium and promoter in the 1Cr0.10A catalyst, leads to an increase in T_{MAX}, due to increase in interaction with the promoter.

The H_2-uptake was also calculated and are mentioned in Table 1. Based on the H_2-uptake and nominal Cr-loading the H/Cr molar ratio was determined and are also included in Table 1. The simultaneous presence of chromium and promoter increases the H/Cr ratio suggesting in an increase in the amount of reducible surface chromium oxide species, except for Na. For the 1Cr0.01Na sample, the amount of reducible chromium oxide species decreases. The 1CrZr catalyst has a H/Cr ratio of 2.69, whereas the H/Cr ratio for 1Cr0.01Na is 2.57. Only the 1Cr0.10K sample has a H/Cr ratio of 3.06, implying that all the chromium oxide species are initially present as Cr^{+6} species and are reducible. The other alkali and alkaline promoters have a H/Cr value less than 3, suggesting the presence of some of chromium oxide species that were difficult to reduce. The H/Cr value less than 3 may be due to Cr^{+3} species strongly interacting with ZrO_2 or those that are strongly interacting with the promoter. The difficult to reduce Cr^{+3} species strongly interacting with the ZrO_2 support were identified in previous XPS study [27]. The H_2-uptake or H/Cr ratio follows the sequence:

$$1Cr0.10K > 1Cr0.10Mg > 1Cr0.10Ca > 1CrZr > 1Cr0.10Na$$

This trend also suggests that the maximum amount of non-reducible chromia species is present in 1Cr0.10Na, followed by 1CrZr, 1Cr0.10Ca and 1Cr0.10Mg. In contrast, there appears to be only reducible Cr^{+6} in the freshly calcined 1Cr0.10K sample.

Table 1: H_2-TPR studies showing the effect of different promoters on 1Cr0.10A catalysts, where A = 0, Na, Mg, K and Ca

Catalyst	T_{MAX} (°C)	H_2-uptake $\left(\frac{mol}{g_{cat}}\right) * 10^6$	H/Cr
1CrZr	305	259	2.69
1Cr0.10Na	313	248	2.57
1Cr0.10Mg	315	281	2.92
1Cr0.10K	308	295	3.06
1Cr0.10Ca	319	273	2.83

The H_2-TPR profile of the second set of catalysts 1CryK, where y = 0.00, 0.05, 0.10, 0.15 and 0.20, is shown in Figure S10 of the supplementary information file. The H_2-TPR profile shows that all the samples continue to exhibit one reduction peak. With the addition of K, T_{MAX} increases, and the specific values are included in Table 2 along with the H_2-uptake and H/Cr molar ratio.

Table 2: H_2-TPR studies showing the effect of different promoters on 1CryK catalyst, where y = 00, 0.05, 0.10, 0.15 and 0.20.

Catalyst	T_{MAX} (°C)	H_2-uptake $\left(\frac{mol}{g_{cat}}\right) * 10^6$	H/Cr
1CrZr	305	259	2.69
1Cr0.05K	307	288	2.99
1Cr0.10K	308	295	3.06
1Cr0.15K	310	301	3.13

1Cr0.20K	312	289	3.00

The addition of K increases the H_2-uptake up to K/Cr = 0.15, and above this value the H_2-uptake starts to decrease. Since the amount of Cr is the same in all samples listed in Table 2, the H/Cr ratio also follows the same trend as H_2-uptake values. In Table 2, the H/Cr values slightly more than 3.00 may be associated with the errors involved in determining the H_2-update and the actual Cr-loading. Despite these minor differences it appears that for this set of catalysts the surface chromia species is predominantly present as Cr^{+6} when K is present.
The H_2-TPR profiles of 1.5CryK and 2.5CryK, where y = 0.00, 0.05, 0.10, 0.15 and 0.20, are shown in Figure S11 and S12 of the supplementary information file and follow a similar trend as 1CryK. The presence of K leads to an increase in T_{MAX} from 301 ℃ to 312 ℃ for 1.5CryK and from 294 ℃ to 306 ℃ for 2.5CryK and the specific values are included in Tables S3 and S4. These tables also show that with the addition of K, the H_2-uptake increases up to a certain value of K/Cr ratio and then the uptake value decreases. The highest H_2-uptake value is achieved at K/Cr of 0.10 for the 1.5CryK samples and at K/Cr of 0.05 for the 2.5 CryK samples. The corresponding H/Cr values for the samples with the highest H_2-uptake are close to 3 for the three series of the samples 1CryK, 1.5CryK and 2.5CryK, which suggests that all the chromium oxide species present on the ZrO_2 support are Cr^{+6} at these K/Cr ratios. These samples are: 1Cr0.15K, 1.5Cr0.10K and 2.5Cr0.05K.
For the last set of catalysts, 2.5CrZr, $2.5Cr_1 0.05K_2$ and $2.5Cr_2 0.05K_1$, the H_2-TPR profiles are shown in Figure S13 of the supplementary information file. In this set of catalysts, the sequence of impregnation methods is compared. The T_{MAX} of the three catalysts vary between 5 ℃ and the specific values are included in Table S5 of the supplementary information file. The amount of H_2-uptake for the catalyst prepared by co-impregnation and sequential impregnation are also within 2%. There is little to distinguish between these three catalysts in terms of T_{MAX}, H_2-uptake and H/Cr ratio; however, they are very different from 2CrZr.

3.6. Reactivity studies

3.6.1. Effect of different promoters

The $X_{C_3H_8}(\%)$ and $Y_{C_3H_8}(\%)$ at 550 ℃ and atmospheric pressure over 1CrZr and 1Cr0.10A are given in Table 3 along with the two TOFs. The H/Cr molar ratio of these samples, given in Table 1, are also included for comparison. The 1Cr0.10K showed the highest activity and TOF among all the 1Cr0.10A samples and the trend is:

$$1Cr0.10K > 1Cr0.10Mg > 1Cr0.10Ca > 1CrZr > 1Cr0.10Na$$

The same trend was observed for the H_2-uptake and H/Cr ratio over these catalysts. It appears that the correlation between the H/Cr ratio and activity holds for the PDH reaction while using different alkali and alkaline promoters. Such a correlation suggests that a larger fraction of Cr^{+6} species in the sample give rise to a more active catalyst during PDH [27].

Table 3: PDH studies over 1CrZr and 1Cr0.10A showing the effect of the addition of different promoters, A = Na, Mg, K and Ca. Reaction conditions: Temperature 550°C, Total pressure = 1 atm, W=100 mg, $W/F_{C3H8,0}$ = 16.59 g.h/mol, $P_{C3H8,0}$ = 0.075 atm, balance N_2. The H/Cr ratio is included for reference.

Catalyst	H/Cr	C_3H_8 Con	C_3H_6 Yiel	$TOF_{C_3H_8}$	$TOF_{C_3H_6}$
1CrZr	2.69	12.89±0.11	11.72±0.05	11.22±0.10	10.20±0.05
1Cr0.10Na	2.57	12.77±0.08	11.09±0.11	10.68±0.07	9.65±0.10
1Cr0.10Mg	2.92	14.30±0.08	13.31±0.15	12.44±0.08	11.59±0.13
1Cr0.10K	3.06	15.42±0.09	15.00±0.20	13.42±0.08	13.05±0.17
1Cr0.10Ca	2.83	13.17±0.06	12.72±0.10	11.46±0.05	11.07±0.08

3.6.2. Effect of Cr-loading on the K/Cr ratio

Since the K promoted catalyst was the best performing, the effect of Cr-loading on the K/Cr ratio is examined for 1CryK, 1.5CryK and 2.5CryK catalysts. The results for the 1CryK catalysts for the PDH reaction is shown in Figure 6. The reaction results show that an increase in K/Cr ratio leads to an initial increase in $X_{C_3H_8}(\%)$ and $Y_{C_3H_8}(\%)$ for the PDH reaction and at a K/Cr ratio of 0.15 the conversion and yield is maximum. The H_2-uptake, H/Cr ratio and TOF for this 1Cr0.15K were also maximum, as shown in in Table S6. Again, there is a strong correlation between the H/Cr ratio and activity of the catalysts during PDH.

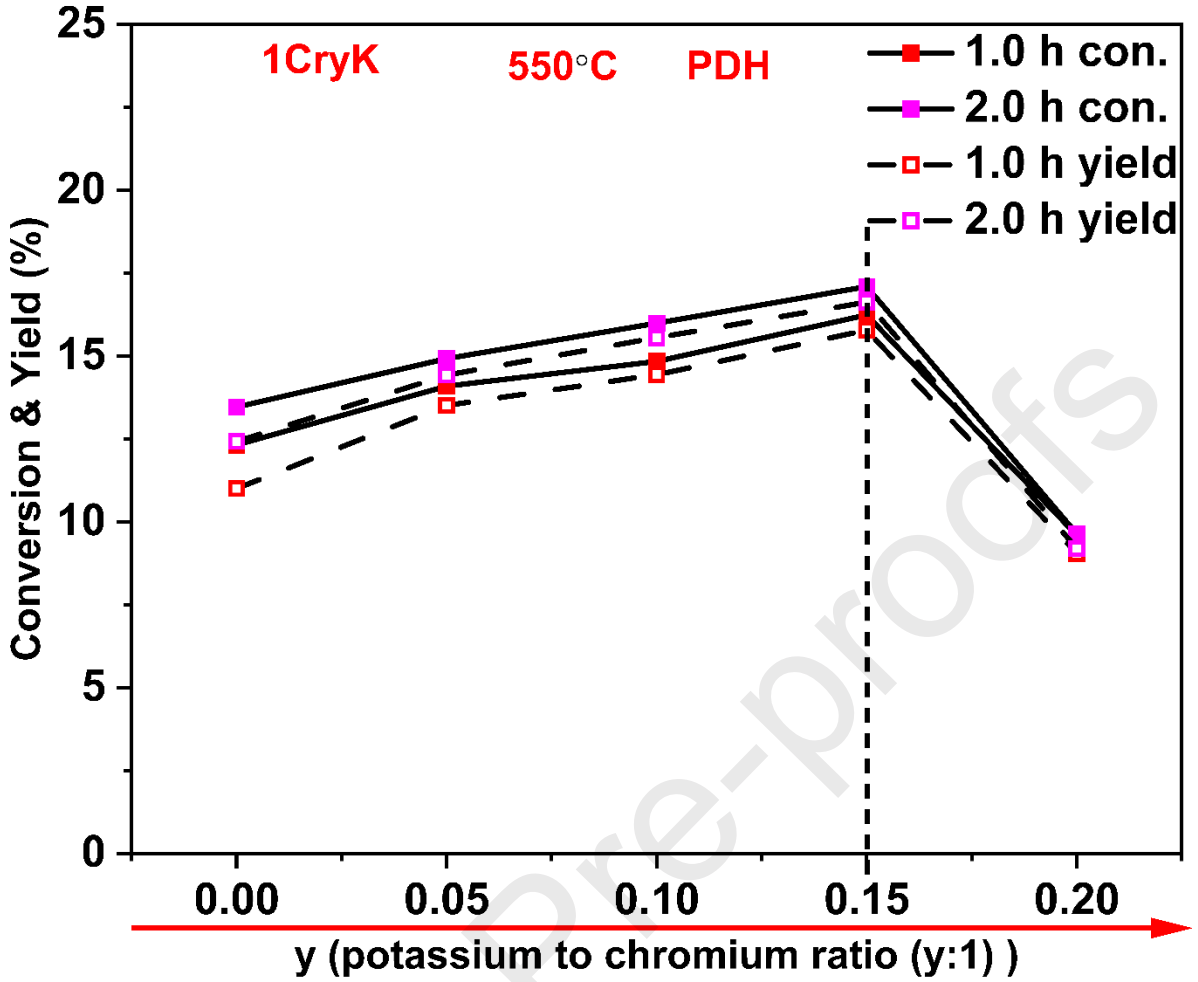

Figure 6: C_3H_8 conversion and C_3H_6 yield for PDH over 1CryK catalysts showing the effect of potassium loading, y = 0.00, 0.05, 0.10, 0.15 and 0.20. Reaction conditions are those mentioned in Table 3.

The reactions result for 1.5CryK, where y = 0.00, 0.05, 0.10 and 0.15 and 0.20, are shown in Figure S14 of the supplementary information file. The catalytic activity improves with an increase in K/Cr ratio up to 0.10 and with a further increase in the ratio the conversion and yield drops. This non-monotonic behaviour of catalytic activity with K/Cr ratio is also seen for the 2.5CryK series of catalysts and the most effective ratio was 0.05. Details of the 2.5CryK series of catalysts are available in our previous study [27] and is provided as Figure S15 in the supplementary information file for convenience. The trend of H_2-uptake, H/Cr ratio and TOFs for 1CryK, 1.5CryK and 2.5CryK are similar. However, the catalytic activity is maximum at different values of K/Cr. The corresponding K/Cr values are 0.15 for 1CryK, 0.10 for 1.5CryK and 0.05 for 2.5CryK, which are mentioned in Tables S6, S7 and S8. Thus, with an increase in Cr-loading, the K/Cr molar ratio of the most active catalyst decreases.

3.6.3. Effect of impregnation sequences

The final set of catalysts was prepared to examine the impregnation sequence of K and Cr on the pre-treated ZrO_2 support. The prepared samples were evaluated for the PDH reaction, and the results are shown in Table 4 along with the H/Cr ratio. Table 4 reveals that all the three catalysts of this set were more active than the unpromoted 2.5CrZr catalyst. Furthermore, the presence of K in supported chromium oxide catalyst increases the H/Cr ratio, bringing it closer to 3, irrespective of the impregnation sequence. Clearly the addition of K increases the amount of the reducible Cr^{+6} species. It appears that the co-impregnated catalyst, 2.5Cr0.05K, is better than the catalysts synthesized by sequential impregnation, $2.5Cr_10.05K_2$ and $2.5Cr_20.05K_1$.

However, the minor differences between the actual Cr/Zr and Cr/K ratios determined by EDS, as shown in Table S2, may play a role in proper comparison between these three catalysts of this set.

Table 4: PDH studies over 2.5CrZr, 2.5Cr0.05K, $2.5Cr_1 0.05K_2$ and $2.5Cr_2 0.05K_1$ catalyst showing the effect of impregnation sequence. Reaction conditions are those mentioned in Table 3. The PDH study over KZr is included for reference.

Catalyst	H/Cr	C_3H_8 C	C_3H_6 Yi	$TOF_{C_3H_8}$	$TOF_{C_3H_6}$
KZr	-	2.30±0.07	1.09±0.03	-	-
2.5CrZr	2.42	16.44±0.16	15.17±0.17	5.72±0.05	5.28±0.06
2.5Cr0.05K	2.95	19.71±0.16	19.06±0.14	6.86±0.05	6.63±0.05
$2.5Cr_1 0.05K_2$	2.89	18.71±0.13	17.48±0.17	6.51±0.05	6.08±0.06
$2.5Cr_2 0.05K_1$	2.89	17.54±0.14	16.66±0.13	6.11±0.05	5.80±0.05

3.7. Causes for promotion

The above results reveal that promotion of the ZrO_2 supported chromium oxide catalyst occurs by increasing the H/Cr ratio to values close to 3. At a H/Cr ratio of 3 all chromium oxide species in the calcined samples are present as Cr^{+6} species and these species are reduced to Cr^{+3} during H_2-TPR. In the unpromoted calcined catalyst the chromium oxide species are present as Cr^{+6} and Cr^{+3}, as shown previously in Figure 3 [27,38]. The Cr^{+3} species present in the calcined catalyst are inactive and are strongly interacting with the ZrO_2 matrix rendering them catalytically inactive. However, in the promoted catalysts containing the optimum amount K/Cr ratio, the K-promoter appear to be preferentially interacting with the ZrO_2 matrix generating ZrO_X species as shown by XPS in Figure 4, and all the chromium oxide species is present as Cr^{+6}. Thereby, the H/Cr ratio increases to 3 and the activity increases since the amount of reducible Cr^{+6} species increases. Such a model explaining the role of K-promoter in the promotion of ZrO_2 supported chromium oxide catalysts, which is illustrated in Figure 7, can also be used to explain the effect of Cr-loading on the K/Cr ratio. For each Cr-loading, an increase in K/Cr ratio results in an increase in catalytic activity and H/Cr ratio up to a value close to 3, and a further increase in K/Cr ratio results in a decrease in H/Cr ratio and catalytic activity.

Interestingly, the amount of K in the three most active catalyst of each Cr-loading, 1Cr0.15K, 1.5Cr0.10K and 2.5Cr0.05K, are similar and correspond to about 0.11 wt.% K. It appears that this is the "saturation amount" of K required for this ZrO_2 support. Amount of K less than this "saturation amount" causes part of the chromium oxide species to be present as Cr^{+3} that strongly interacts with the ZrO_2 matrix. Furthermore, K amounts more than the "saturation amount" gives rise to K being available for chromium oxide to form a compound, which are not reducible and is inactive. Consequently, the H/Cr ratio and catalytic activity decreases, and an optimum K/Cr ratio is achieved.

Potassium containing chromia oxide compounds, such as $K_2Cr_2O_7$ and K_2CrO_4, are common. In these two compounds, chromium is present as Cr^{+6}, which cannot be readily differentiated from the surface molecularly dispersed Cr^{+6} species by UV-vis, but these species are visible and it is differentiated in Cr XPS spectra of 2.5Cr0.05K catalysts. Consequently, the UV-vis spectra would not change, which is seen in the present study in Figures S1 to S5. It is also possible that for each alkali and alkaline promoter chosen, the "saturation amount" is different and a more detailed study might have provided a more complete understanding. Furthermore, the presence of Cr^{+6} and Cr^{+3} in unpromoted supported catalysts are also seen or proposed with other supports [9,32,42]. The "saturation amount" for each of these supports for the alkali and alkaline promoters may also be different. It is left for future studies to explore these effects in more detail.

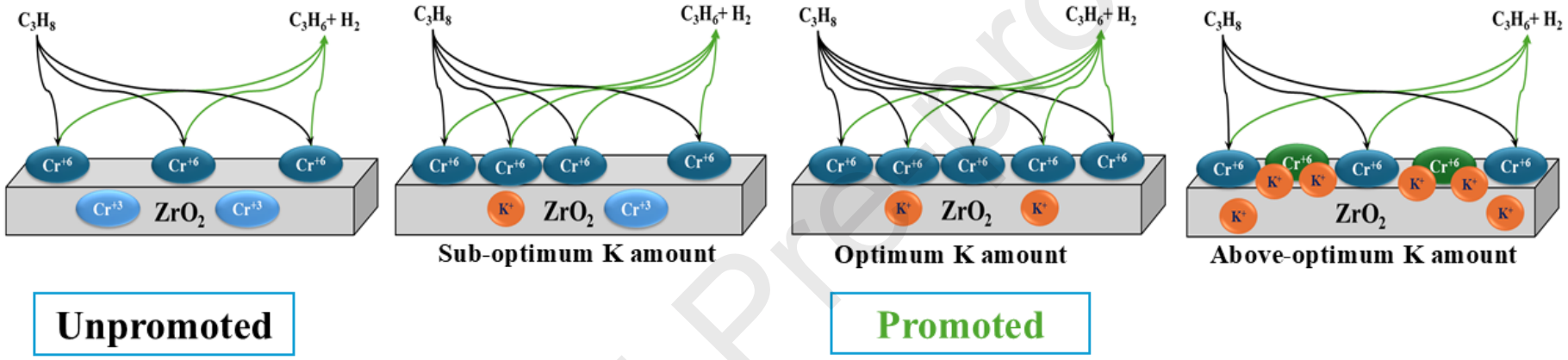

Figure 7: A model showing the effect of potassium promotion for ZrO_2 supported chromium oxide catalysts.

3.8. Regeneration study

The most active catalyst, 2.5Cr0.05K, was chosen to study the catalyst stability and its ability to regenerate over several oxidation-reduction cycles, and the results are shown in Figure 8. It is evident that the C_3H_6 yield initially increases and then starts decreasing almost linearly with TOS. The selectivity of C_3H_6 is initially ~98% and after that it stays around 99% or more for all cycles. Similar deactivation results are also seen for a Al_2O_3 supported chromia catalyst [32].

For the 2.5Cr0.05K catalyst the yield decreases to about 45% of its initial value for Cycle I after 6 h TOS. After regeneration the next cycle was initiated. For all cycles, the initial C_3H_6 yield, its increase and subsequent decrease were similar. However, the amount of deactivation for Cycles III, IV and V progressively decreased. After about a 45% decrease in C_3H_6 yield for Cycles I and II, the decrease in C_3H_6 yield was about 25% for Cycle III, 19% for Cycle IV and 21 % for Cycle V. Despite these differences, it is evident that 2.5Cr0.05K has an excellent ability to be regenerated over several cycles.

The spent and regenerated 2.5Cr0.05K samples were collected from regeneration study after each cycle. The Raman spectra of the samples collected after cycles I, III and V are shown in Figure 9. It is evident that the carbon bands are absent for the regenerated catalysts of all catalysts. Furthermore, the spent catalyst after 6 h of TOS show distinct Raman bands due to carbon deposited on the surface. These Raman bands appear to decrease in intensity with the increase in number of cycles. Thus, the deactivation of the catalysts in different cycles are due to carbon formation, and this deposited carbon can be completely removed by calcination at 550°C.

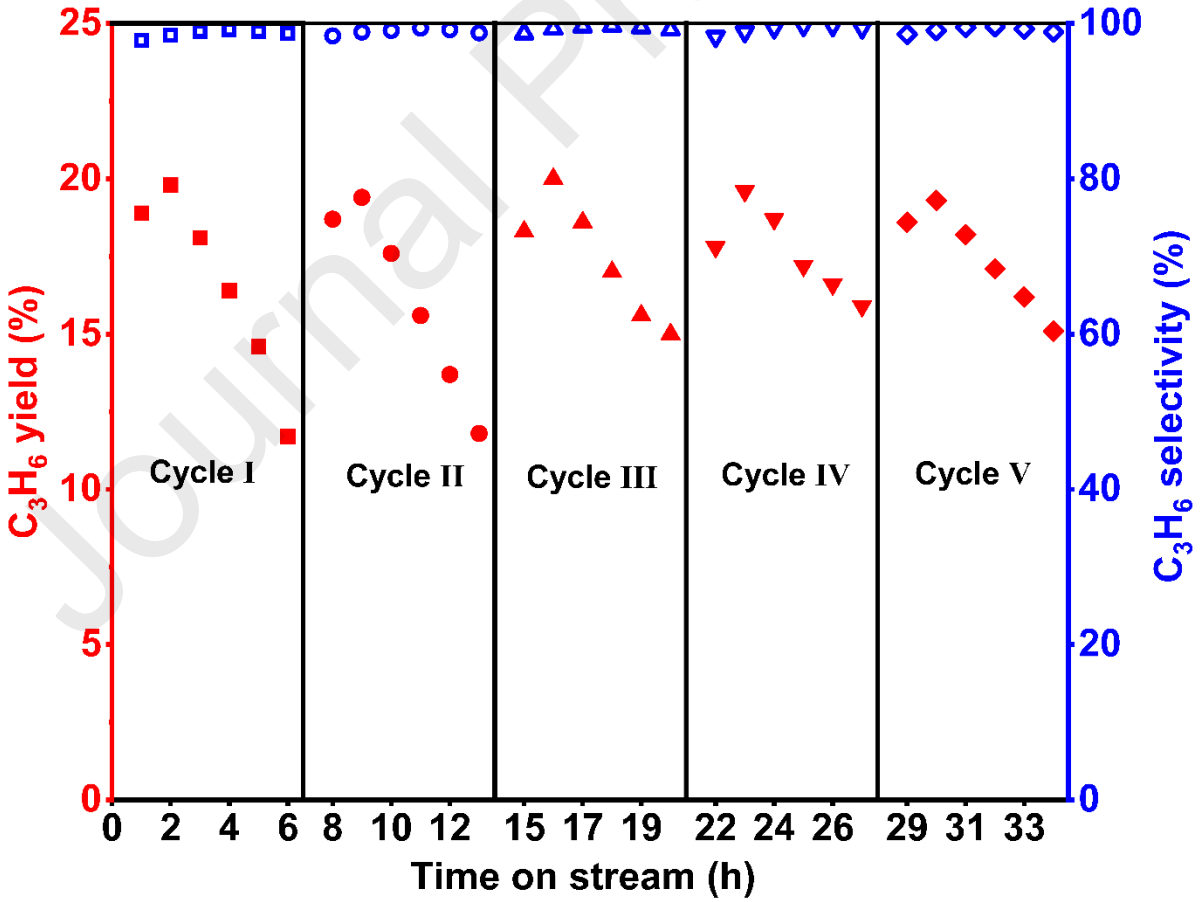

Figure 8: Regeneration study over 2.5Cr0.05K catalyst during the PDH reaction at different TOS. Reaction conditions are those mentioned in Table 3.

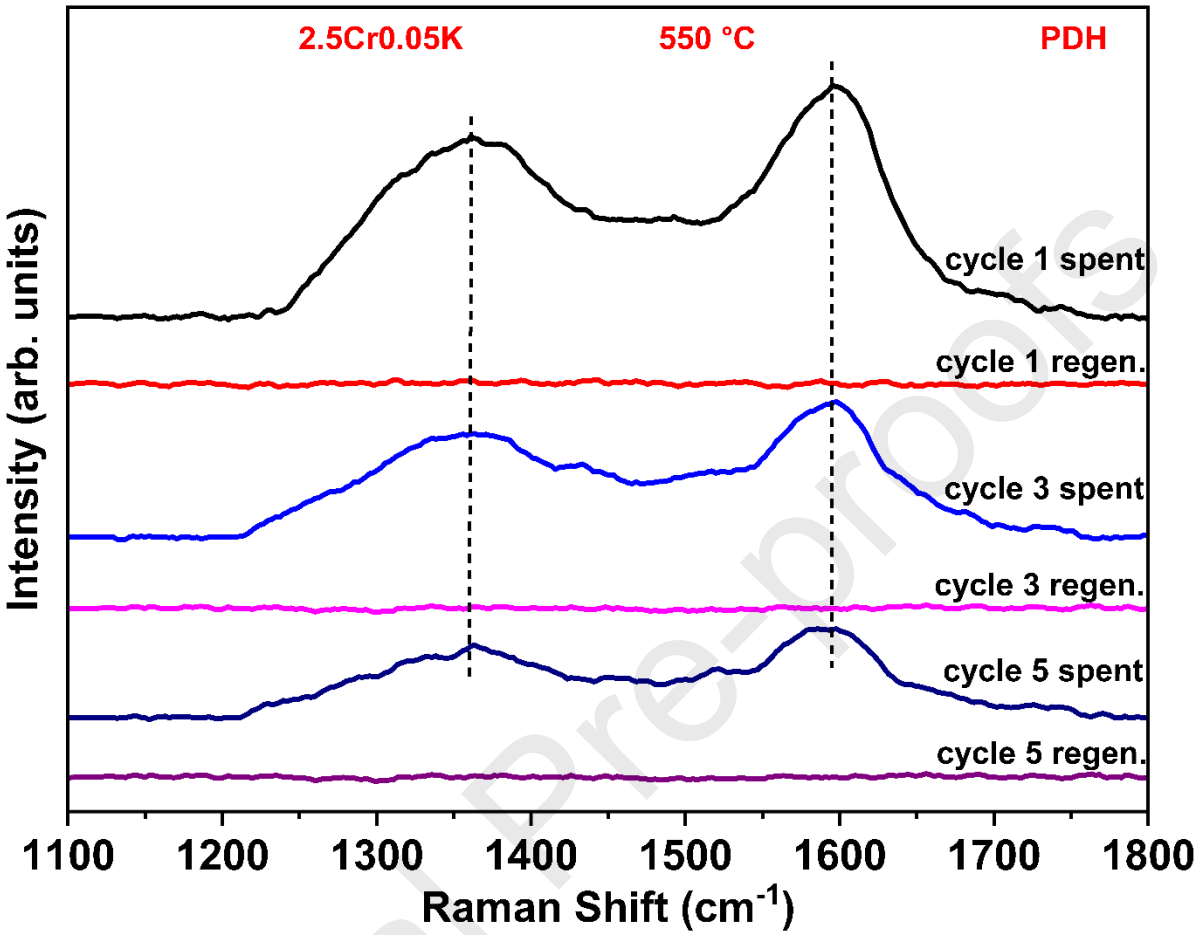

Figure 9: Raman spectra of the spent and regenerated 2.5Cr0.05K catalysts during PDH reaction at 550 °C, after different cycles 1, 3 and 5. The spent spectra was obtained on the catalyst after 6 h of reaction.

3.8. Contact time studies of PDH and CO_2-ODH

To improve the catalytic activity further, the contact time (W/F_{A0}, $g_{cat}.h/mol$) for carrying out the PDH reaction was varied for 2.5Cr0.05K. The CO_2-ODH reaction over the same catalyst using the same contact times and inlet partial pressure of C_3H_8 was also carried out and the results of both reactions are compared in Figure 10. Furthermore, the inlet partial pressures of CO_2 and C_3H_8 were the same for the CO_2-ODH reaction. Figure 10 shows that the conversion and yield of C_3H_8 and C_3H_6 monotonically increase and then appear to approach a constant value when the contact time was increased about 10 times from 3.76 to 37.33 $g_{cat}.h/mol$. For CO_2-ODH, the conversion of CO_2 and yield of CO for CO_2-ODH reaction are shown in Figure S16 of the supplementary information file. Figure S16 shows that the trend in CO_2 conversion and CO yield is similar to the conversion and yield of C_3H_8 and C_3H_6. It appears that during CO_2-ODH two parallel reaction pathways (PDH and RWGS) occur simultaneous on the surface Cr sites. Consequently, on some of the Cr sties RWGS takes place, which leads to a decrease in PDH activity [38]. Figure 10 also shows that the conversion of C_3H_8 and the yield of C_3H_6 for PDH is always better than that for CO_2-ODH under the same conditions. The $X_{C_3H_8}(\%)$and $Y_{C_3H_8}(\%)$ achieved for the PDH reaction at a contact time of 37.33 $g_{cat}.h/mol$ and temperature of 550 °C were ~30% and ~27%, respectively. In contrast,

the $X_{C_3H_8}(\%)$ and $Y_{C_3H_8}(\%)$ during CO_2-ODH under identical conditions were 17.5 % and 15.5 %, respectively. Furthermore, with an increase in contact time, the difference between conversion and yield increases, suggesting carbon growth.

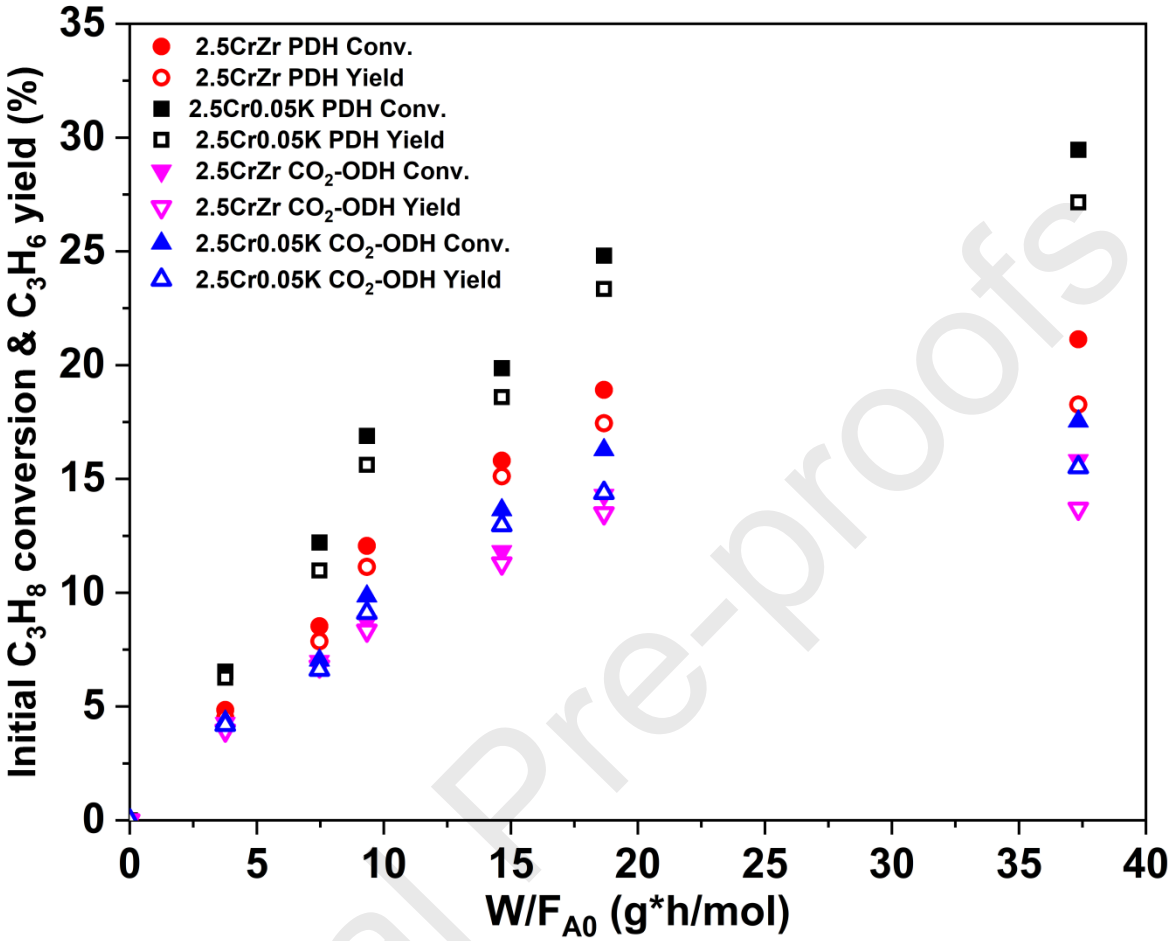

Figure 10: C_3H_8 conversion and C_3H_6 yield for the PDH and CO_2 ODH over 2.5CrZr and 2.5Cr0.05K catalyst showing the effect of contact time. Reaction conditions: Temperature 550°C, Total pressure = 1 atm, W=100 mg, $W/F_{C3H8,0}$ = 0.00-37.33 $g_{cat}\,.h/mol$.

Previous studies have reported the catalytic performance of Cr-based PDH catalysts, and selected examples are summarized in Table S9 of Supplementary Information file. The catalytic evaluations were conducted under broadly comparable reaction conditions (550 °C and atmospheric pressure). As shown in the table, the Cr loading varies significantly (2.5-20 wt.%), primarily depending on the nature of the support material. Similarly, the reported GHSV values range from 3800 to 18,000 mL g_{cat}^{-1} h^{-1}. Notably, the optimized catalyst developed in the present study exhibits one of the lowest Cr loadings (2.5 wt.%) while operating at the highest GHSV (18,000 mL g_{cat}^{-1} h^{-1}). Despite these comparatively stringent operating conditions, the catalytic performance of the present catalyst remains highly competitive with those reported in the literature.

4. Conclusion

In the present study, we initially investigated the effect of various alkali and alkaline earth metal promoters (Na, Mg, K, and Ca) on chromia-supported zirconia (CrZr) catalysts for the PDH reaction. The K-promoted catalysts exhibited superior activity compared to those promoted with Na, Mg, and Ca. The H/Cr ratio was also the highest for the K-promoted sample.

For different Cr-loading, the K/Cr molar ratio for the best catalyst was different. It was 0.15 for 1CrZr, 0.10 for 1.5CrZr, and 0.05 for 2.5CrZr. The H/Cr ratio of these catalysts were the highest in each series and approached a value of 3. A value of 3 corresponds to all the supported chromium oxide species being in the Cr^{+6} state, which can be reduced to Cr^{+3} during H_2 treatment or the PDH reaction. The impregnation sequence of K and Cr does not appear to have an effect on the catalyst properties and catalytic activity. The amount of K present in the best catalyst for each Cr-loading is ~0.11 wt.% K, which we refer to as the "saturation amount" of K for this ZrO_2 support. Amounts of K less than the saturation amount results in some of the chromium oxide species being present as inactive Cr^{+3} species; whereas K amounts more than saturation amounts give rise to Cr^{+6}-K compounds that are also inactive. Thus, an optimum amount of K/Cr ratio is required to maintain the surface chromium oxide species as active and reducible Cr^{+6} species. The ability of the best catalyst, 2.5Cr0.05K, to regenerate was also examined, and excellent reusability was seen. Contact times studies showed that the PDH reaction consistently outperformed the CO_2-assisted oxidative dehydrogenation (CO_2-ODH) for C_3H_6 production, for the given conditions. The C_3H_8 conversion and C_3H_6 yield for PDH were 30% and 27% and 17.5% and 15.5% for CO_2-ODH at a contact time of 37.33 g_{cat}.h/mo $l_{C_3H_8}$ and 550 °C. Future studies may consider generalizing the similarity and differences of the two reactions.

Supplementary Information

The Supporting Information includes detailed characterization data for the Cr-containing catalysts, comprising BET surface area analysis, EDX, UV-vis spectroscopy, Raman spectroscopy, XPS, and H_2-TPR measurements. Additionally, catalytic performance data for the Cr-containing catalysts and a contact time study for the 2.5Cr0.05K catalyst are provided.

Acknowledgement

The authors acknowledge the Indian Institute of Technology Kanpur and the Ministry of Education (MoE), Government of India, for continued support. Rajvikram Singh additionally acknowledges financial support from the FARE Fellowship, IIT Kanpur.

References

[1] U. Department of Energy, Chapter 6: Innovating Clean Energy Technologies in Advanced Manufacturing, 2015.

[2] F.E. Frey, W.F. Huppke, Equilibrium Dehydrogenation of Ethane, Propane, and the Butanes, UTC, 2025. https://pubs.acs.org/sharingguidelines.

[3] S. Chen, X. Chang, G. Sun, T. Zhang, Y. Xu, Y. Wang, C. Pei, J. Gong, Propane dehydrogenation: Catalyst development, new chemistry, and emerging technologies, Chem. Soc. Rev. 50 (2021) 3315–3354. https://doi.org/10.1039/d0cs00814a.

[4] J.H. Carter, T. Bere, J.R. Pitchers, D.G. Hewes, B.D. Vandegehuchte, C.J. Kiely, S.H. Taylor, G.J. Hutchings, Direct and oxidative dehydrogenation of propane: From catalyst design to industrial application, Green Chemistry 23 (2021) 9747–9799. https://doi.org/10.1039/d1gc03700e.

[5] G. Wang, X. Zhu, C. Li, Recent Progress in Commercial and Novel Catalysts for Catalytic Dehydrogenation of Light Alkanes, Chemical Record 20 (2020) 604–616. https://doi.org/10.1002/tcr.201900090.

[6] M. Monai, M. Gambino, S. Wannakao, B.M. Weckhuysen, Propane to olefins tandem catalysis: A selective route towards light olefins production, Chem. Soc. Rev. 50 (2021) 11503–11529. https://doi.org/10.1039/d1cs00357g.

[7] F. Cabrera, D. Ardissone, O.F. Gorriz, Dehydrogenation of propane on chromia/alumina catalysts promoted by tin, Catal. Today 133–135 (2008) 800–804. https://doi.org/10.1016/j.cattod.2007.12.039.

[8] J. Liu, Y. Liu, Y. Ni, H. Liu, W. Zhu, Z. Liu, Enhanced propane dehydrogenation to propylene over zinc-promoted chromium catalysts, Catal. Sci. Technol. 10 (2020) 1739–1746. https://doi.org/10.1039/c9cy01921a.

[9] P.P. Li, W.Z. Lang, K. Xia, L. Luan, X. Yan, Y.J. Guo, The promotion effects of Ni on the properties of Cr/Al catalysts for propane dehydrogenation reaction, Appl. Catal. A Gen. 522 (2016) 172–179. https://doi.org/10.1016/j.apcata.2016.05.007.

[10] Y. Zhang, S. Yang, J. Lu, Y. Mei, D. He, Y. Luo, Effect of a Ce Promoter on Nonoxidative Dehydrogenation of Propane over the Commercial Cr/Al2O3 Catalyst, Ind. Eng. Chem. Res. 58 (2019) 19818–19824. https://doi.org/10.1021/acs.iecr.9b03870.

[11] H. Shao, X. Wang, X. Gu, D. Wang, T. Jiang, X. Guo, Improved catalytic performance of CrOx catalysts supported on foamed Sn-modified alumina for propane dehydrogenation, Microporous and Mesoporous Materials 311 (2021). https://doi.org/10.1016/j.micromeso.2020.110684.

[12] J. Ma, H. Yuan, C. Liu, J. Wang, R. Zhang, A. Ma, Enhanced propane dehydrogenation performance using bimetallic-modified GaPt/SiO2-Al2O3 with ultralow-loading Pt, Fuel 369 (2024). https://doi.org/10.1016/j.fuel.2024.131788.

[13] J. Zhou, H. Liu, C. Xiong, P. Hu, H. Wang, X. Wang, H. Ji, Potassium-promoted Pt–In bimetallic clusters encapsulated in silicalite-1 zeolite for efficient propane dehydrogenation, Chemical Engineering Journal 455 (2023). https://doi.org/10.1016/j.cej.2022.139794.

[14] L. Cai, Y. Zhao, X. Tian, D. Qin, C. Wei, X. Cai, W. Chu, W. Yang, Well-dispersed monolayer CrOx/Silicalite-1 catalysts for efficient propane dehydrogenation, Chemical Engineering Journal 494 (2024). https://doi.org/10.1016/j.cej.2024.152925.

[15] Q. Li, J. Zhang, T. Yu, J. Chen, G. Wang, Z. Shi, R. Zhuo, R. Wang, Advanced metal oxide catalysts for propane dehydrogenation: from design strategy to dehydrogenation performance, Nanoscale (2025). https://doi.org/10.1039/d4nr04482g.

[16] J. Fang, J. Lu, B. He, Z. Xu, M. Luo, T. Song, H. Wang, C. Qin, Z. Chen, Y. Luo, Identification of the Potassium-Related Species as the Key Active Sites for C-S Bond Couplings over K-MoS2 Materials, ACS Catal. 14 (2024) 11604–11616. https://doi.org/10.1021/acscatal.4c02672.

[17] J.H. Carter, T. Bere, J.R. Pitchers, D.G. Hewes, B.D. Vandegehuchte, C.J. Kiely, S.H. Taylor, G.J. Hutchings, Direct and oxidative dehydrogenation of propane: From catalyst design to industrial application, Green Chemistry 23 (2021) 9747–9799. https://doi.org/10.1039/d1gc03700e.

[18] R. Singh, J.K. Prabhakar, G. Deo, K-Promotion Enhances the Intrinsic Kinetics of Fe/ZrO_2 Catalysts for the RWGS Reaction, Energy & Fuels 40 (2026) 9603–9614. https://doi.org/10.1021/acs.energyfuels.6c01012.

[19] E. Rombi, M.G. Cutrufello, V. Solinas, S. De Rossi, G. Ferraris, A. Pistone, Effects of potassium addition on the acidity and reducibility of chromia/alumina dehydrogenation catalysts, Appl. Catal. A Gen. 251 (2003) 255–266. https://doi.org/10.1016/S0926-860X(03)00308-9.

[20] S. Han, T. Otroshchenko, D. Zhao, H. Lund, U. Rodemerck, D. Linke, M. Gao, G. Jiang, E. V. Kondratenko, Catalytic non-oxidative propane dehydrogenation over promoted Cr-Zr-Ox: Effect of promoter on propene selectivity and stability, Catal. Commun. 138 (2020). https://doi.org/10.1016/j.catcom.2020.105956.

[21] J.J.H.B. Sattler, I.D. González-Jiménez, A.M. Mens, M. Arias, T. Visser, B.M. Weckhuysen, Operando uv-vis spectroscopy of a catalytic solid in a pilot-scale reactor: Deactivation of a crox/al2o3 propane dehydrogenation catalyst, Chemical Communications 49 (2013) 1518–1520. https://doi.org/10.1039/c2cc38978a.

[22] F. Cavani, M. Koutyrev, F. Trifirò, A. Bartolini, D. Ghisletti, R. Iezzi, A. Santucci, G. Del Piero, Chemical and Physical Characterization of Alumina-Supported Chromia-Based Catalysts and Their Activity in Dehydrogenation of Isobutane, 1996.

[23] D. Liu, P. Bai, P. Wu, D. Han, Y. Chai, Z. Yan, Surface chemistry and catalytic performance of chromia/alumina catalysts derived from different potassium impregnation sequences, Appl. Surf. Sci. 351 (2015) 250–259. https://doi.org/10.1016/j.apsusc.2015.05.128.

[24] S. De Rossi, G. Ferraris, S. Fremiotti, V. Indovina, A. Cimino, Isobutane dehydrogenation on chromia/zirconia catalysts, 1993.

[25] S. De Rossi, M.P. Casaletto, G. Ferraris, A. Cimino, G. Minelli, Chromia/zirconia catalysts with Cr content exceeding the monolayer. A comparison with chromia/alumina and chromia/silica for isobutane dehydrogenation, n.d.

[26] T.P. Otroshchenko, U. Rodemerck, D. Linke, E. V. Kondratenko, Synergy effect between Zr and Cr active sites in binary CrZrOx or supported CrOx/LaZrOx: Consequences for catalyst activity, selectivity and durability in non-oxidative propane dehydrogenation, J. Catal. 356 (2017) 197–205. https://doi.org/10.1016/j.jcat.2017.10.012.

[27] R. Singh, R. Singh, G. Deo, Developing a supported metal oxide catalyst for direct dehydrogenation of propane to propene, Appl. Catal. A Gen. 703 (2025). https://doi.org/10.1016/j.apcata.2025.120354.

[28] A. Węgrzyniak, A. Rokicińska, E. Hędrzak, B. Michorczyk, K. Zeńczak-Tomera, P. Kuśtrowski, P. Michorczyk, High-performance Cr-Zr-O and Cr-Zr-K-O catalysts prepared by nanocasting for dehydrogenation of propane to propene, Catal. Sci. Technol. 7 (2017) 6059–6068. https://doi.org/10.1039/c7cy01744h.

[29] M.G. Cutrufello, S. De Rossi, I. Ferino, R. Monaci, E. Rombi, V. Solinas, Preparation, characterisation and activity of chromia-zirconia catalysts for propane dehydrogenation, in: Thermochim. Acta, 2005: pp. 62–68. https://doi.org/10.1016/j.tca.2005.01.017.

[30] H. Shao, Q. He, D. Wang, Y. Zhang, T. Jiang, X. Guo, The active sites and catalytic properties of CrOx/Zn-Al2O3 catalysts for propane dehydrogenation, Appl. Catal. A Gen. 637 (2022). https://doi.org/10.1016/j.apcata.2022.118610.

[31] H. Karami, S. Soltanali, M. Amanati, W. Song, J. Liu, K. Sharifi, The promotion effects of alkaline earth metals on the properties of Cr/η-Al2O3 catalysts for propane dehydrogenation, Journal of Saudi Chemical Society 28 (2024). https://doi.org/10.1016/j.jscs.2024.101929.

[32] H. Fu, W. Qian, H. Zhang, H. Ma, W. Ying, Different alkali metals promoted Cr/Al2O3 catalysts for propane dehydrogenation, Fuel 342 (2023). https://doi.org/10.1016/j.fuel.2023.127774.

[33] P. Michorczyk, P. Pietrzyk, J. Ogonowski, Preparation and characterization of SBA-1-supported chromium oxide catalysts for CO 2 assisted dehydrogenation of propane, Microporous and Mesoporous Materials 161 (2012) 56–66. https://doi.org/10.1016/j.micromeso.2012.05.011.

[34] Isao Takahara, Masahiro Saito, Promoting Effects of Carbon Dioxide on Dehydrogenation of Propane over a SiO2-supported Cr2O3 Catalyst, Chemistry Letters, Volume 25, Issue 11, November 1996, 25, 973–974, https://doi.org/10.1246/cl.1996.973

[35] R. Wu, P. Xie, Y. Cheng, Y. Yue, S. Gu, W. Yang, C. Miao, W. Hua, Z. Gao, Hydrothermally prepared Cr2O3-ZrO2 as a novel efficient catalyst for dehydrogenation of propane with CO2, Catal. Commun. 39 (2013) 20–23. https://doi.org/10.1016/j.catcom.2013.05.002.

[36] M.A. Atanga, F. Rezaei, A. Jawad, M. Fitch, A.A. Rownaghi, Oxidative dehydrogenation of propane to propylene with carbon dioxide, Appl. Catal. B 220 (2018) 429–445. https://doi.org/10.1016/j.apcatb.2017.08.052.

[37] Y. Gambo, S. Adamu, A.A. Abdulrasheed, R.A. Lucky, M.S. Ba-Shammakh, M.M. Hossain, Catalyst design and tuning for oxidative dehydrogenation of propane – A review, Appl. Catal. A Gen. 609 (2021). https://doi.org/10.1016/j.apcata.2020.117914.

[38] R. Singh, S.C. Nayak, R. Singh, G. Deo, O2 and CO2 assisted oxidative dehydrogenation of propane using ZrO2 supported vanadium and chromium oxide catalysts, Catal. Today 432 (2024). https://doi.org/10.1016/j.cattod.2024.114617.

[39] J.F.S. de Oliveira, D.P. Volanti, J.M.C. Bueno, A.P. Ferreira, Effect of CO2 in the oxidative dehydrogenation reaction of propane over Cr/ZrO2 catalysts, Appl. Catal. A Gen. 558 (2018) 55–66. https://doi.org/10.1016/j.apcata.2018.03.020.

[40] S.S. Chan, I.E. Wachs, L.L. Murrell, L. Wang, W.K. Hall, In Situ Laser Raman Spectroscopy of Supported Metal Oxides, 1984. https://pubs.acs.org/sharingguidelines.

[41] T. V. Malleswara Rao, G. Deo, J.M. Jehng, I.E. Wachs, In situ UV-Vis-NIR diffuse reflectance and raman spectroscopy and catalytic activity studies of propane oxidative dehydrogenation over supported CrO 3/ZrO 2 catalysts, Langmuir 20 (2004) 7159–7165. https://doi.org/10.1021/la049590v.

[42] M. Cherian, M.S. Rao, A.M. Hirt, I.E. Wachs, G. Deo, Oxidative dehydrogenation of propane over supported chromia catalysts: Influence of oxide supports and chromia loading, J. Catal. 211 (2002) 482–495. https://doi.org/10.1006/jcat.2002.3759.

[43] C.L. Pieck, M.A. Bañares, J.L.G. Fierro, Propane oxidative dehydrogenation on VOx/ZrO2 catalysts, J. Catal. 224 (2004) 1–7. https://doi.org/10.1016/j.jcat.2004.02.024.

[44] M.G. Cutrufello, S. De Rossi, I. Ferino, R. Monaci, E. Rombi, V. Solinas, Preparation, characterisation and activity of chromia-zirconia catalysts for propane dehydrogenation, in: Thermochim. Acta, 2005: pp. 62–68. https://doi.org/10.1016/j.tca.2005.01.017.

[45] S. Han, T. Otroshchenko, D. Zhao, H. Lund, N. Rockstroh, T.H. Vuong, J. Rabeah, U. Rodemerck, D. Linke, M. Gao, G. Jiang, E. V. Kondratenko, The effect of ZrO2 crystallinity in CrZrOx/SiO2 on non-oxidative propane dehydrogenation, Appl. Catal. A Gen. 590 (2020). https://doi.org/10.1016/j.apcata.2019.117350.

[46] Z. Liu, L. Zhang, S. Ren, Y. Zhao, S. Agathopoulos, H. Lu, B. Peng, L. Yin, L. Deng, Stability and reactivity of zirconium diboride in intermediate-temperature hydrothermal conditions: A comprehensive analysis, Mater. Today Commun. 41 (2024). https://doi.org/10.1016/j.mtcomm.2024.110482.

[47] P. Bouvier, G. Lucazeau, Raman spectra and vibrational analysis of nanometric tetragonal zirconia under high pressure, n.d. www.elsevier.nl/locate/jpcs.

[48] E. Rombi, D. Gazzoli, M.G. Cutrufello, S. De Rossi, I. Ferino, Modifications induced by potassium addition on chromia/alumina catalysts and their influence on the catalytic activity for the oxidative dehydrogenation of propane, Appl. Surf. Sci. 256 (2010) 5576–5580. https://doi.org/10.1016/j.apsusc.2009.12.151.

[49] P.G. Harrison, N.C. Lloyd, W. Daniell, The nature of the chromium species formed during the thermal activation of chromium-promoted tin(iv) oxide catalysts: an epr and xps study, Journal of Physical Chemistry B 102 (1998) 10672–10679. https://doi.org/10.1021/jp9822135.

[50] Y. Zhao, D. Chen, J. Liu, D. He, X. Cao, C. Han, J. Lu, Y. Luo, Tuning the metal-support interaction on chromium-based catalysts for catalytically eliminate methyl mercaptan: Anchored active chromium species through surface hydroxyl groups, Chemical Engineering Journal 389 (2020). https://doi.org/10.1016/j.cej.2020.124384.

[51] Y. Zhao, J. Lu, D. Chen, L. Zhang, S. He, C. Han, D. He, Y. Luo, Probing the nature of active chromium species and promotional effects of potassium in Cr/MCM-41 catalysts for methyl mercaptan abatement, New Journal of Chemistry 43 (2019) 12814–12822. https://doi.org/10.1039/c9nj02858g.

[52] C. Chantharangsi, S. Denchitcharoen, S. Chaiyakun, P. Limsuwan, Structures, morphologies, and chemical states of sputter-deposited CrZrN thin films with various Zr contents, Thin Solid Films 589 (2015) 613–619. https://doi.org/10.1016/j.tsf.2015.06.045.

[53] R. Camposeco, S. Castillo, N. Nava, R. Zanella, Boosting of Soot Combustion on Alkaline Mn/ZrO2 Nanostructures, Top. Catal. 63 (2020) 481–491. https://doi.org/10.1007/s11244-020-01224-z.

Highlights

- K promoter is better than Na, Ca and Mg for Cr/ZrO_2 and catalyst can be regenerated
- Optimum K/Cr molar ratio varies with Cr loading, while K % on ZrO_2 is the same

- Changing sequence of impregnation of Cr and K on ZrO_2 results in similar catalysts
- K interacts with ZrO_2 forming low-valent ZrO_X sites and releasing irreducible Cr^{+3}
- Propene yield for PDH reaction is better than for CO_2-ODH at all contact times

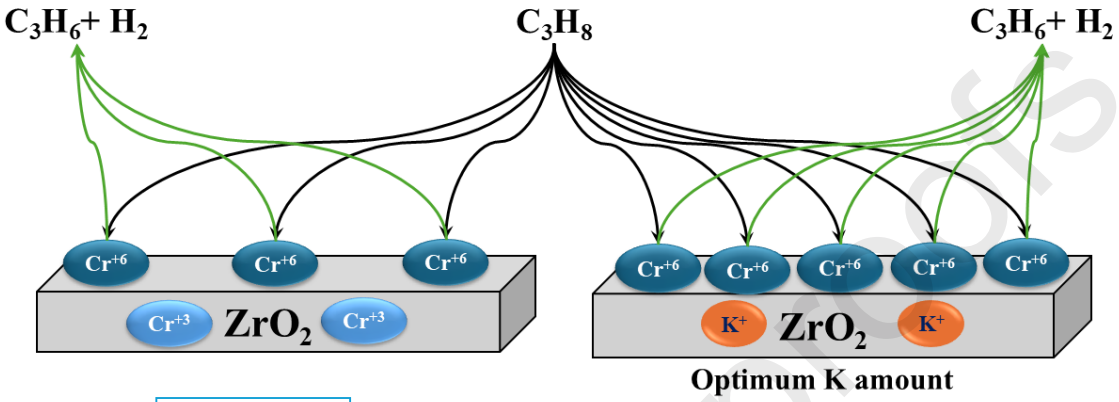

Saturation amount of K for ZrO_2 = 0.11 wt.%
PDH shows better activity than CO_2-ODH

Declaration of interests

☒ The authors declare that they have no known competing financial interests or personal relationships that could have appeared to influence the work reported in this paper.

☐ The authors declare the following financial interests/personal relationships which may be considered as potential competing interests: